Fig. S1

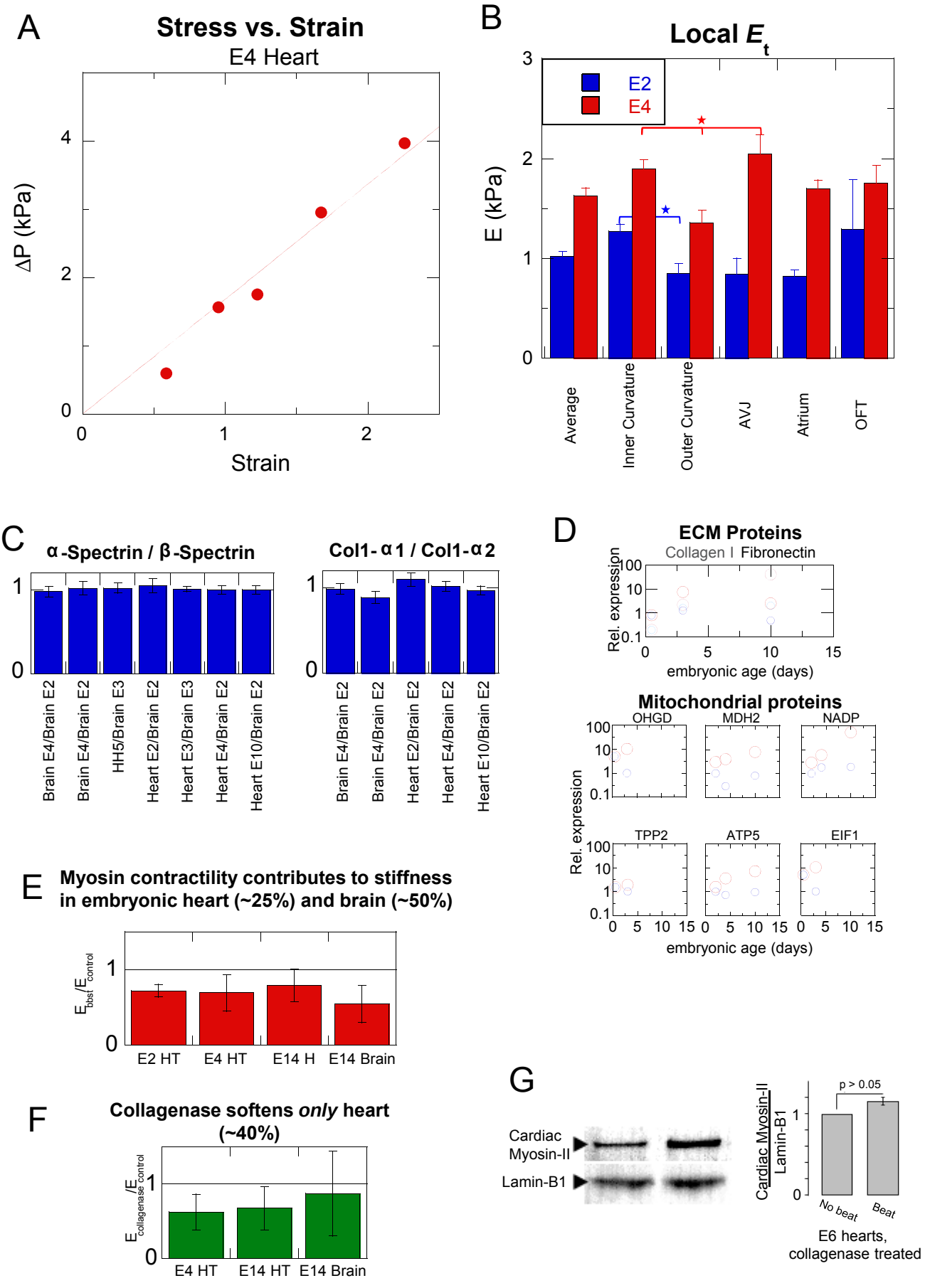
A
Stress vs. Strain
E4 Heart
ΔP (kPa)
Strain
B
Local E_t
E2
E4
E (kPa)
Average
Inner Curvature
Outer Curvature
AVJ
Atrium
OFT
C
α-Spectrin / β-Spectrin
Col1-α1 / Col1-α2
Brain E4/Brain E2
Brain E4/Brain E2
HH5/Brain E3
Heart E2/Brain E2
Heart E3/Brain E3
Heart E4/Brain E2
Heart E10/Brain E2
D
ECM Proteins
Collagen I
Fibronectin
Rel. expression
embryonic age (days)
Mitochondrial proteins
OHGD
MDH2
NADP
TPP2
ATP5
EIF1
E
Myosin contractility contributes to stiffness in embryonic heart (~25%) and brain (~50%)
E2 HT
E4 HT
E14 H
E14 Brain
F
Collagenase softens *only* heart (~40%)
E4 HT
E14 HT
E14 Brain
G
Cardiac Myosin-II
Lamin-B1
p > 0.05
No beat
Beat
E6 hearts, collagenase treated

Fig. S2

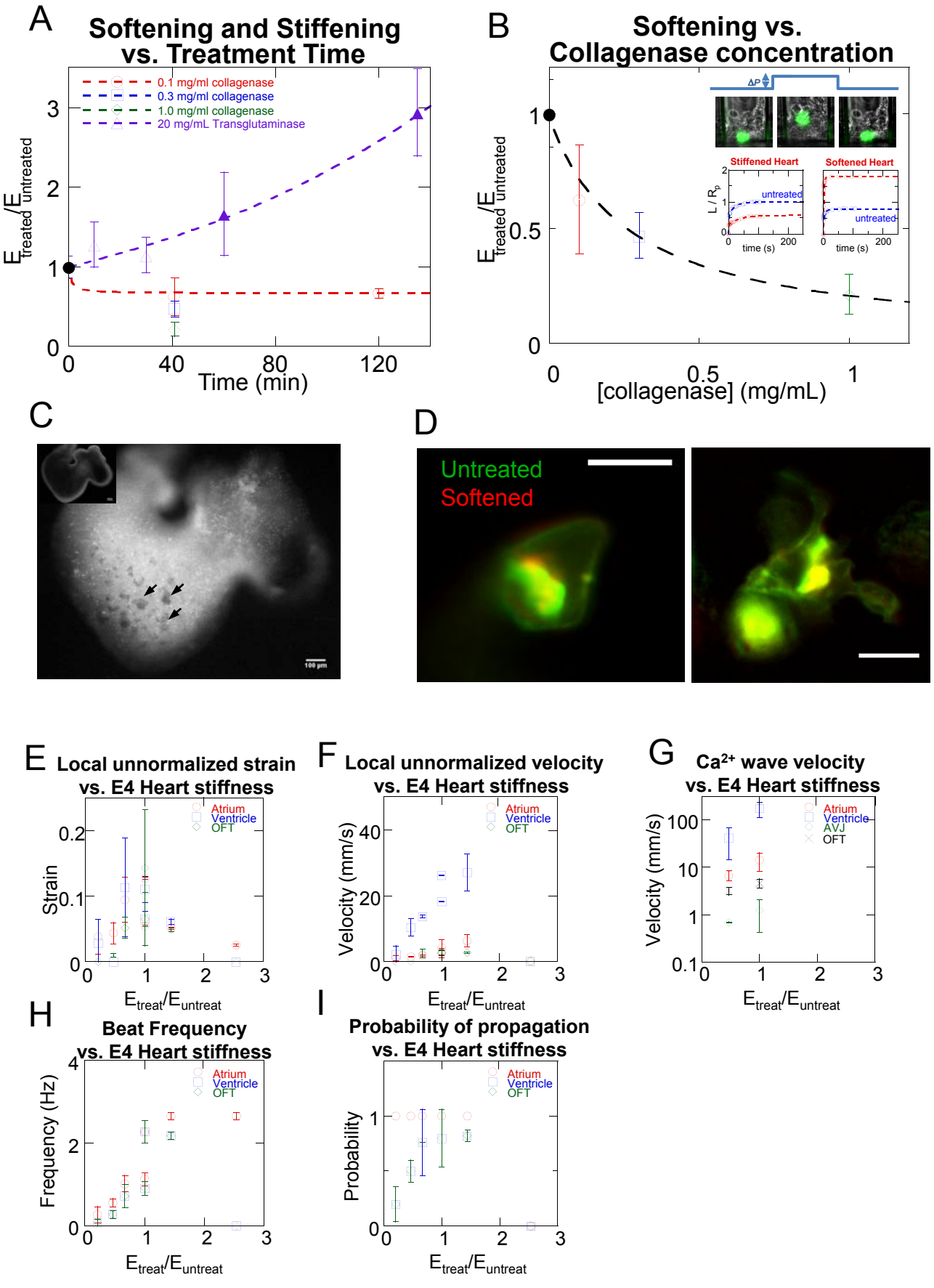
A
Softening and Stiffening vs. Treatment Time
0.1 mg/ml collagenase
0.3 mg/ml collagenase
1.0 mg/ml collagenase
20 mg/mL Transglutaminase
E treated/E untreated
Time (min)
B
Softening vs. Collagenase concentration
ΔP
Stiffened Heart
Softened Heart
untreated
L / Rp
time (s)
E treated/E untreated
[collagenase] (mg/mL)
C
D
Untreated
Softened
E
Local unnormalized strain vs. E4 Heart stiffness
Atrium
Ventricle
OFT
Strain
Etreat/Euntreat
F
Local unnormalized velocity vs. E4 Heart stiffness
Velocity (mm/s)
G
Ca2+ wave velocity vs. E4 Heart stiffness
AVJ
H
Beat Frequency vs. E4 Heart stiffness
Frequency (Hz)
I
Probability of propagation vs. E4 Heart stiffness
Probability

Fig. S3

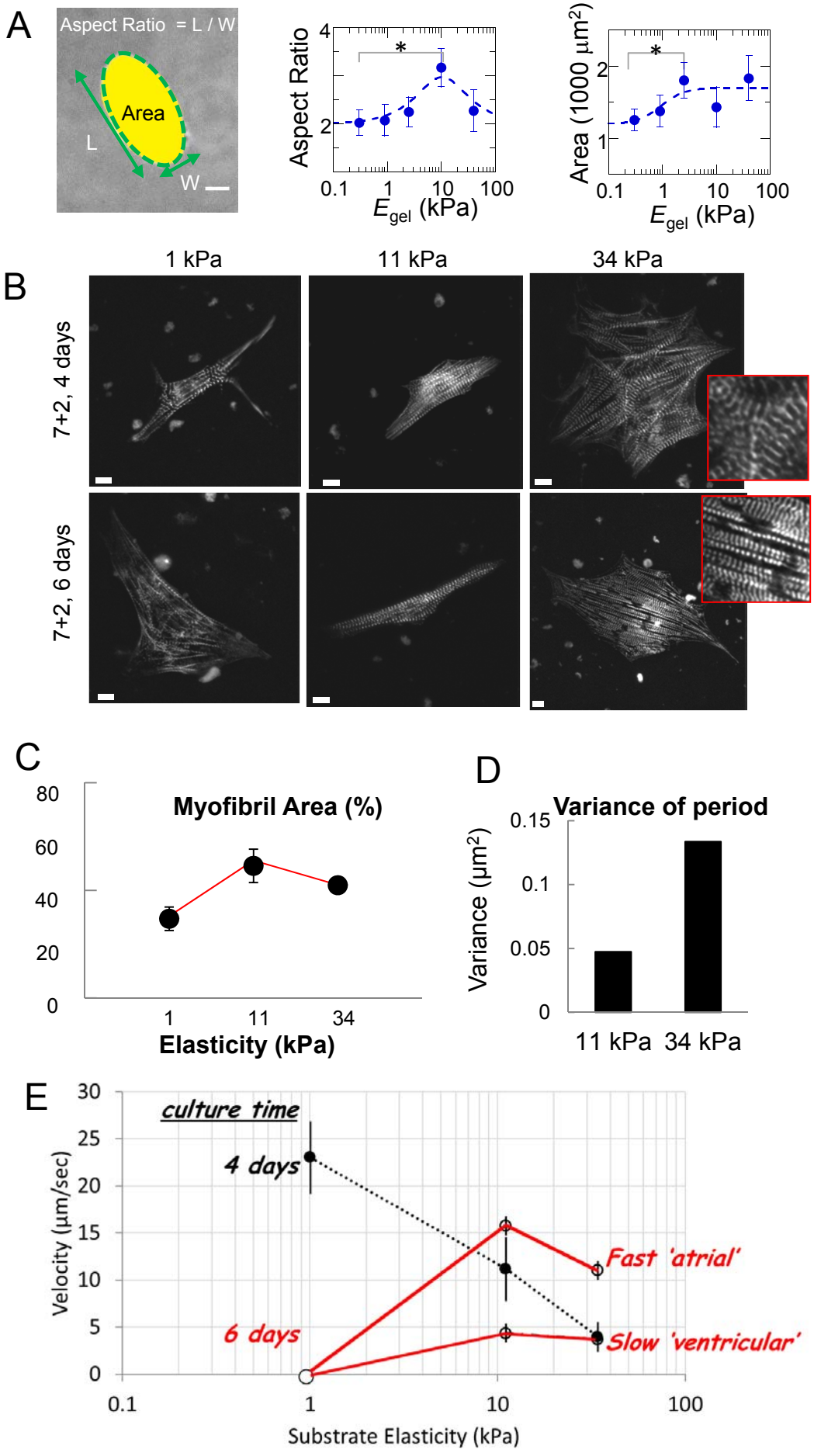
A
Aspect Ratio = L / W
Area
L
W
Aspect Ratio
E_{gel} (kPa)
Area (1000 μm²)
E_{gel} (kPa)
B
1 kPa
11 kPa
34 kPa
7+2, 4 days
7+2, 6 days
C
Myofibril Area (%)
Elasticity (kPa)
D
Variance of period
Variance (μm²)
11 kPa 34 kPa
E
culture time
4 days
6 days
Fast 'atrial'
Slow 'ventricular'
Velocity (μm/sec)
Substrate Elasticity (kPa)

Supplemental Figure Legends

Fig. S1. Related to Figure 1 and Table S1. Anatomically distinct mechanics of embryonic tissue can be softened differentially by disrupting cytoskeleton or collagenous matrix. (A) Example Stress/Strain curve of an E4 Heart Tube ventricle. From Eq. 1, E_t = 1.7 ± 0.1 kPa. (B) Anatomical differences in E_t are measured along the E2-E4 heart tubes that reflect functional developmental changes (AVJ = atrioventricular junction, OFT = outflow tract). (C) As a check for the protein quantification, we compared the relative amounts of α and β Spectrins and Col Ia1 and Ia2. Since these spectrins and collagens should normally be found at ratios of 1:1 and 2:1, respectively, their normalized abundances should be equal across all samples, which is what we find. (D) Of the two ECM proteins identified, Collagen-I and Fibronectin, only Collagen follows the trends of the tissue mechanics. Several mitochondrial proteins were also identified to follow the trends of the tissue mechanics, but generally not as strongly and at a lower abundance than the excitation-contraction coupling proteins discussed in the text. (E) Treatment of E2, E4 and E14 heart and E14 brain (5 measurements each of n = 4, 4, 2, 2, respectively) with blebbistatin softens the tissues significantly, allowing us to estimate of the contribution of actomyosin contractile forces to tissue mechanics (~25% for heart and ~50% for brain). (F) Treatment of E4 and E14 heart and E14 brain (5 measurements each of n = 4, 2, 3, respectively) with collagenase shows that a significant softening of the heart tissue (~ 40%), but no softening of the brain tissue. Due to the thick epicardial layer of E4 heart, the softening of myocardium due to collagenase is likely underestimated. (G) Immunoblot of E6 hearts treated for 50 min with collagenase that had stopped beating (n = 3) and continued beating (n = 2) shows no significant difference in myosin expression. Error bars are ± SEM (n ≥ 3 unless indicated).

Fig. S2. Related to Figure 2 and Movie S1. Effects of dose-dependent stiffening and softening of E4 embryonic cardiac tissue by transglutaminase and collagenase on intact tissue structure and function. *(A*) Change in tissue stiffness as a function of treatment time with 20 mg/mL transgluatminase (purple triangles, filled triangles represent the intermediate and extreme stiffening treatments used in the strain and velocity measurements) and different concentrations of collagenase (red circles 0.1 mg/mL, blue squares 0.3 mg/mL, green diamonds 1.0 mg/mL). Treatment with transglutaminase leads to stiffening whereas collagenase treatment softens the tissue. (B) Softening of tissue as a function of collagenase concentration for 30 min treatments. We assume the collagenase acts with Michaelis-Menten kinetics, so fit the data with $\frac{E_{treated}}{E_{untreated}} = \frac{a}{b+[collagenase]}$, finding a = 0.26±0.08 mg/ml and b = 0.27±0.1 mg/ml. Inset shows aspiration and relaxation of a 0.1 ml/mg collagenase softened E4 HT tissue including a GFP-expressing cell, demonstrating that individual cells return to their original shape and position upon relaxation from applied strain. Also in inset are sample aspiration curves for tissues before (blue) and after (red) softening and stiffening. (C) After 30 min, fluorescently labeled collagenase perfusion of an E4

HT shows that the tissue is fully perfused with the enzyme. Black arrows indicate possible trabeculae. (D) Overlays of SIRPA-GFP expression by transfected cells in beating E4 HTs before (green) and after (red) collagenase treatment show that treatment does not significantly alter cell membrane contour and thus likely does not significantly interfere with cell adhesions. (E) Un-normalized strain and (F) velocity measured from analysis of fluorescent imaging of GFP-transfected heart tubes that have been softened or stiffened. (G) Ca2+ wave velocity in untreated and softened heart tubes. The Ca2+ imaging allowed for more precise localization of the Ca2+ wave than the strain wave, so the atrioventricular junction (AVJ) could be differentiated from the atrium and ventricle. The strain wave velocity measurements across the atrium and ventricle were made from the initiation of contraction to the AVJ and then from the AVJ to points in the presumptive right ventricle, respectively. Therefore the strain wave atrium and ventricle include time from the AVJ and so are measured to be slower than the Ca^{2+} wave. The Ca^{2+} wave is coincident with the initiation of contraction in the heart, and therefore shows the same trends in velocity as the strain wave with softening. (H) Beat frequency in each chamber decreases with softening and does not significantly change with stiffening, except in the stiffest condition in which the contraction wave does not propagate past the atrium. (I) Similarly, probability of contraction propagating decreases with softening but does not significantly change with slight stiffening and drops to zero in the extreme stiffening condition.

Fig. S3. Related to Figure 3. Changes in E4 cardiomyocyte aspect ratio and area during contraction are optimized by intermediate substrate stiffness. (A) Cell aspect ratio and area, schematized at left, are significantly modulated by substrate elasticity. The peak in cell aspect ratio fits a Lorentzian (see Supplement Box 1) peaked at E_m = 10 ± 4 kPa, whereas cell area fits a generalized Hill equation with a mid-point of 2 ± 1 kPa. (B) Representative images of ESC-CM stained for a-actinin to visualize z-discs after being cultured on soft, intermediate, and stiff substrates for 4 days. (D,E,F) Representative image of ESC-CM after 6 days cultured on elastic substrates. Defects reminiscent of disclinations and dislocations in liquid crystals (upper inset) and cracks (lower inset) arise in the myofibril organization of ESC-CM cultured on stiff substrates. (C) Mature myofibril content quantified by % of total cell area is maximized on intermediate stiffness substrates after 4 days in culture. Myofibril content decreases further in cells grown on soft substrates and is maintained in intermediate to stiff substrates (data not shown). (D) Mature myofibril spacing of cells cultured on stiff substrates shows increased variance relative to that of cells grown on intermediate substrates. (E) Edge velocities of spontaneously beating ESC-CM cultured for 4 and 6 days on soft, intermediate, and stiff substrates. After just 4 days, edge velocity decreases with increasing stiffness, reflecting the increased load that the beating cell feels on different substrates. After 6 days, ESC-CM stop beating on the softest substrates, and two populations can be seen on the intermediate and stiff substrates, indicating possible further differentiation into fast-contracting “atrial” type cells and slow-contracting “ventricular” type cells.

Movie S1. Related to Figure 2 and Figure S2, and supplemental experimental methods. Effects of stiffening or softening collagenous ECM on E4 HT beating. Movies of E4 HT beating in culture shown in the following order: (1) Phase contrast and (2) fluorescent imaging of a GFP transfected E4 HT. (3) Fluorescent imaging of Ca^{2+} in a Fluo-4 loaded E4 HT.

Table S1. Related to Figure 1, Figure S1, and supplemental experimental methods. Mass-Spec of early and late embryonic brain and heart tissue. Heat map of all identified proteins from two experiments: E2, E4, and E10 Heart and Brain tissue normalized to E2 Brain, and HH3-5 embryonic disc and E3 heart and brain normalized to E3 Brain. Proteins are clustered by the Manhattan Distance algorithm. Grey cells indicate undetected proteins for that experiment.

Box 1. ***Friedrich-Safran Model of Matrix Elasticity optimized Registration Force: a Functional form***

Since striation is central to contractile function of any heart or skeletal muscle, a mathematical model of striation can help clarify striation mechanisms as well as processes dependent on striation, particularly the contractile strains measured here. Friedrich et al. (2011) account for matrix elasticity effects and force generation in calculating how striated contractile fibers in cells on elastic substrates interact with each other and come into maximal registry on substrates of intermediate stiffness [16]. The myosin-II based contractile force that drives myofibril registry in the Friedrich-Safran (FS) model follows a non-monotonic form $f \sim E / (E_m + E)^2$ with a maximum at $E = E_m$. Striation organization dynamics in simulations were quantified in terms of a registration order parameter (i.e. 'smectic' order), and fit f^n

$$Striation \sim [\, E / (E_m + E)^2 \,]^n \qquad \text{(Eqn. 1)}$$

with n decreasing exponentially over time from $n \approx 1$ to 0.6. Importantly, high n gives a sharper peak at half-max than low n. Moreover, because non-striated cardiomyocytes do not beat, striation is also key to rhythmic strains that we measured in tissue and isolated cells. Matrix strain in cultures of sparse cells indeed fit well to Eq.1 with an optimal elasticity $E_m = 1.3 \pm 0.3$ kPa and $n = 1$ (Fig. 3B). This result is particularly remarkable because f is relatively restrictive, with only one fitting parameter. For the intact heart, Eq.1 also fits the measured strain with $E_m = 1.6 \pm 0.2$ kPa but with $n = 4 \pm 1$ (Fig. 2C). The higher exponent quantifies the much sharper peak for tissue, indicating a greater sensitivity to matrix elasticity in tissue compared to cells in sparse 2D cultures.

Box 2. ***Mechanical Signaling Model for Contractile Waves***

Based only on Excitation-Contraction Coupling, the contractile wavefront speed should not depend on matrix elasticity. The excitable medium model here is linear in E_t: cells are coupled mechanically through extracellular matrix and cell contractions are triggered by mechanosensitive means, namely Excitation-Contraction-Matrix Coupling (see Supplement). The heart tube is considered per a two-fluid model [27] with isotropic linear elasticity (matrix plus cells) of elasticity E and Poisson ratio ν as well as tissue viscosity η. Damping forces couple viscous and elastic components through a coupling constant Γ.

$$\Gamma\left(\partial_t u_i - v_i\right) = \frac{E}{2(1+\nu)}\left(\partial_k \partial_k u_i + \frac{1}{1-2\nu}\partial_i \partial_k u_k\right) + \partial_j Q_{ij}\delta(\vec{x})\Theta(t)\Theta(\Delta t - t)$$

$$\Gamma\left(\partial_t u_i - v_i\right) = -\eta \partial_k \partial_k v_i + \partial_i p$$

$$0 = \partial_k v_k$$

Here $\delta(x)$ is the Dirac delta function, $\Theta(t)$ the Heaviside step function, and Δt the duration of the contraction. The wavefront speed depends on two material parameters: an effective "diffusion constant" $D = E / \Gamma$, and a relaxation time $\tau = 2\,\eta\,(1+\nu) / E$. A predicted threshold value of $E_0 = 0.1E_{untreat}$, below which the system is too soft to support a contractile wavefront, is consistent with observations that – with softening treatments – the contraction wave failed to propagate sometimes into the ventricular region, which is softer than the atrium (Fig S1B). The probability of propagating indeed decreased monotonically with softening (Fig. S2I). Failure to propagate when $E > E_o$ could be due to inhomogeneities in stiffness. Intriguingly, the stiffness of embryonic heart when it first begins to beat at E2 is also roughly $0.1E_{adult}$ (Fig. 1C), which is several-fold stiffer than the embryonic disc.

Supplemental Analysis

Mechanical Signaling Model for Contractile Waves

It is well recognized in biological contexts such as *Dictyostelium* [S7] that chemical signaling can proceed via propagating wavefronts if a local increase in concentration of some chemical species can trigger further release of that species at that same location, thus amplifying the signal. Analogously, we propose that *mechanical* signaling can proceed via the propagation of nonlinear *contractile* wavefronts through mechanically excitable heart tissue. When a cell contracts, it exerts a stress on the surrounding tissue. We approximate this stress as a dipole that conserves the volume of the contracting cell by expanding it perpendicular to the contraction. We denote the strength of the dipoles by Q. Note that tissue itself cannot sustain mechanical (sound) waves because they are damped out exponentially. However, a wave can be maintained if it is continually amplified. In our model, we assume that each cell contracts once the local stress exceeds a certain threshold value α. This could occur, for example, if calcium release is triggered by stress [S8, S9]. By contracting, a cell adds stress to the system, thus amplifying the signal. This mechanism can lead to a wavefront that moves at constant velocity down the heart tube.

More precisely, we treat the heart tube as a two-fluid model [S10]. We model the tissue as having an elastic component (in matrix plus cells) that obeys isotropic linear elasticity and is characterized by the Young's modulus E and Poisson ratio ν. The tissue also has a viscous component that obeys the Stokes equation, is characterized by a viscosity η and is incompressible. Damping forces couple the viscous and elastic components of the material through a coupling constant Γ.

$$\begin{aligned} \Gamma\left(\partial_t u_i - v_i\right) &= \frac{E}{2(1+\nu)}\left(\partial_k\partial_k u_i + \frac{1}{1-2\nu}\partial_i\partial_k u_k\right) + \partial_j Q_{ij}\delta(\vec{x})\Theta(t)\Theta(\Delta t - t) \\ \Gamma\left(\partial_t u_i - v_i\right) &= -\eta\partial_k\partial_k v_i + \partial_i p \\ 0 &= \partial_k v_k \end{aligned} \qquad (2)$$

Here $\delta(x)$ is the Dirac delta function, $\Theta(t)$ the Heaviside step function, and Δt the duration of the contraction. The wavefront speed depends on two material parameters: an effective "diffusion constant" $D = E / \Gamma$, and a relaxation time $\tau = \eta / \mu = 2\eta(1+\nu)/E$, where μ is the material's shear modulus. Additionally, the speed depends on two dimensionless parameters: the Poisson ratio ν and the rescaled threshold $\underline{\alpha} = a^3 \alpha / Q$, where a is the spacing between the cells. By purely dimensional considerations, there are two ways to construct a quantity with the dimensions of a speed: D/a and a/τ. Because both scale linearly with E, we can immediately conclude that the wavefront speed v should

scale with E as well. We have confirmed this by solving the model numerically. A full dimensional analysis shows that $v \sim E\, a^{1-2n}\, \Gamma^{-n}\, \eta^{-(1-n)}$, where n is a number between 0 and 1 that depends on the dimensionless parameters v and $\underline{\alpha}$. For fixed Poisson ratio $v = 0.4$, which is reasonable for soft tissues [S4], we found numerically that n depends strongly on the dimensionless threshold stress $\underline{\alpha}$, increasing from 0.2 for $\underline{\alpha} = 0.5$ to 0.4 for $\underline{\alpha} = 0.75$. At sufficiently high values of $\underline{\alpha}$, or equivalently, sufficiently low values of E, the tissue becomes too soft to trigger cells to contract; below that threshold (which we denote by E_0) the wavefront can fail to propagate ($v=0$).

Pipette aspiration measurements show the ventricle has an effective viscosity $\eta \approx 25$ Pa·s, and since this changes by only 20% for the stiffened and softened tissues, we treat it as constant. The coupling constant Γ is estimated by assuming the largest contribution arises from the relative motion of the cytoskeleton with respect to the cytoplasm. Therefore $\Gamma \sim \eta/x^2$, where x is the displacement during contraction, which we take to be 5 μm, or half the radius of the cell, so that $\Gamma \sim 1$ Pa·s / (μm)^2. We find $\underline{\alpha}$ by fitting the numerical results to the slope of the (E, v) data for the ventricle, which is 13 mm/(kPa·s), and the one-parameter fit yields $\underline{\alpha} \approx 0.5$. The threshold for initiating contractions is thus about half the force per unit volume exerted by the cells themselves while contracting.

Supplemental Experimental Procedures

Tissue isolation White Leghorn chicken eggs (Charles River Laboratories) were incubated at 37˚C, rotated once per day, until the desired developmental stage was reached. Embryos were extracted at room temperature by windowing eggs, removing extraembryonic membranes with forceps and cutting major blood vessels to the embryonic disc tissue to free the embryo. The embryo was placed in a dish containing PBS and quickly decapitated. For E2-E5 embryos, whole heart tubes were extracted by severing the conotruncus and sino venosus. For older embryos, whole hearts were extracted by severing the aortic and pulmonary vessels and the pericardium was sliced and teased away from the ventricle using extra-fine forceps . Brain tissue was collected from the presumptive midbrain. Embryonic discs were removed by windowing the egg, cutting out the embryo with the overlying vitelline membrane intact, lifting out the embryo adherent to the vitelline membrane and placing in a dish of PBS. Extraembryonic tissue was carefully cut away using dissection scissors and the finally embryo was teased away from the vitelline membrane using forceps. All tissues were incubated at 37˚C in pre-warmed chick heart media (alpha-MEM supplemented with 10 % FBS and 1% penn-strep, Gibco, 12571-063) until ready for use.

Mass-Spectrometry of tissues For proteomic studies, tissue of interest was washed three times by successive resuspension in ice-cold PBS and diced to sub-millimeter pieces. Proteins were solubilized by cellular disruption with a probe sonicator in ice-cold RIPA buffer with 0.1% protease inhibitor cocktail (approx. 5000 cells / µL). NuPage LDS sample buffer (Invitrogen) with 1% β-mercaptoethanol was added to 1x concentration, followed by heating to 80°C for 10 min. Proteins were separated on SDS-PAGE gels (NuPAGE 4-12% Bis-Tris, Invitrogen), run at 100 V for 10 min followed by 25 min at 160 V. Sections of excised polyacrylamide gel (cut in two molecular weight ranges: 55-100 kDa and 100-300 kDa) were washed (50% 0.2 M ammonium bicarbomate (AB) solution, 50% acetonitrile, 30 min at 37 °C), dried by lyophilization, incubated with a reducing agent (20 mM tris(2-carboxyethyl)phosphine in 25 mM AB solution at pH 8.0, 15 min at 37°C) and alkylated (40 mM iodoacetamide in 25 mM AB solution at pH 8.0, 30 min at 37 °C). The gel sections were dried by lyophilization before in-gel trypsinization (20 µg/mL sequencing grade modified trypsin in buffer as described in the manufacturer's protocol (Promega Corp. Madison, WI), 18 hr at 37°C with gentle shaking). Before analysis, peptide solutions were acidified by addition of 50% digest dilution buffer (60 mM AB solution with 3% methanoic acid).

Peptide separations (5 µL injection volume) were performed on 15-cm PicoFrit column (75 µm inner diameter, New Objective) packed with Magic 5 µm C18 reversed-phase resin (Michrom Bioresources) using a nanoflow high-pressure liquid chromatography system (Eksigent Technologies), which was coupled online to a hybrid LTQ-Orbitrap XL mass spectrometer (Thermo Fisher Scientific) via a nanoelectrospray ion source. Chromatography was performed with Solvent A (Milli-Q water with 0.1% formic acid) and Solvent B (acetonitrile with 0.1% formic acid). Peptides were eluted at 200 nL/min for 3–28% B over 42 min, 28–50% B over 26 min, 50–80% B over 5 min, 80% B for 4.5 min before returning to 3% B over 0.5 min. To minimize sample carryover, a fast blank gradient was run between each sample. The LTQ-Orbitrap XL operated in the data-dependent mode to automatically switch between full scan MS (m/z = 350-2000 in the orbitrap analyzer with resolution of 60,000 at m/z 400) and fragmentation of the six most intense ions by collision-induced dissociation in the ion trap mass analyzer.

Raw mass spectroscopy data was processed using Elucidator (version 3.3, Rosetta Biosoftware, Cambridge, MA). The software was set up to align peaks in data from samples derived from the same ranges of molecular weight. Peptide and protein annotations were made using SEQUEST (Thermo Fisher Scientific) with full tryptic digestion and up to 2 missed cleavage

sites. Peptide masses were selected between 800 and 4500 amu with peptide mass tolerance of 1.1 amu and fragment ion mass tolerance of 1.0 amu. Peptides were searched against a database compiled from UniRef100 human (for proteomic studies, downloaded 05-Nov-2010) or UniRef100 gallus gallus (for matrix studies, downloaded 12-Jan-2011), plus contaminants and a reverse decoy database. Search results were selected with a deltaCn filter of 0.01 and mass error better than 20 ppm. Ion currents of oxidized peptides (Δ = +15.995 Da) were summed with their parent peptide; post-translational modifications of phosphorylation (Δ = +79.966 Da), acetylation (Δ = +42.011 Da) and methylation (Δ = +14.016 Da) were entered in the search. In matrix studies, we additionally looked for hydroxylation of proline, asparagine, aspartic acid, and lysine (Δ = +15.995 Da).

The two MW ranges of the proteomic dataset were analyzed separately. In the mid-MW range (55-100 kDa), the false-positive (FP) detection rate was estimated to be 11.4% (based on search hits of the decoy database) and only proteins with two-or-more peptides/protein were considered for further analysis (2015 peptides from 231 unique proteins). High-MW range (100-300 kDa): FP rate = 11.3%; subsequent analysis of 1223 peptides from 55 unique proteins. Label free relative peptide quantitation was performed with in-house software coded for Mathematica (Wolfram Research, Champaign, IL). Datasets were normalized against optimized housekeeping peptide sets that were found to be invariant between experimental conditions. A peptide-set optimization algorithm (PRF, [S1]) was used to select peptides that show a similar 'fingerprint' behavior between samples, and these peptides were used for the basis of quantification and normalization. We report only quantification of proteins with at least three PRF peptides/protein (total 178 proteins). Peptides from regions common to several proteins or isoforms were treated distinctly. Standard errors were calculated from at least 2 technical repetitions. As a further check of the peptide selection algorithm, ratio comparisons were made between all datasets and checked for consistency (for example, when considering data A, B and C, the ratio A:B should be consistent with A:C x C:B).

Sample preparation, gel electrophoresis and immunoblotting. Frozen whole embryo (Hamburger-hamilton stage 5-8, n = 4) and tissue from E4, E6, and E14 chick heart (n = 4, 2, and 1, respectively) and brain (n = 3, 2, and 1, respectively) diced to approximately 10 mm^3, was suspended in ice-cold 1x NuPAGE LDS buffer (Invitrogen; 1% protease inhibitor cocktail, 1% β-mercaptoethanol) and subjected to sonication on ice (3 x 15 x 1s pulses, intermediate power setting). Samples were then heated to 80 °C for 10 min and centrifuged at maximum speed for 10 min. SDS-PAGE gels were loaded with 5 – 15 µL of lysate per lane (for LMNB1: NuPAGE 4-12% Bis-Tris, for MYH6: NuPAGE 3-8% Tris-Acetate; Invitrogen). Each sample was loaded in triplicate for averaging purposes. Additionally, sample concentrations were adjusted to match LMNB1 signal whilst avoiding overloading and smearing, diluting the lysates with additional 1x NuPAGE LDS buffer if necessary. Gel electrophoresis was run for 10 min at 100 V and 1 hr at 160 V. After blotting on a polyvinylidene fluoride membrane with an iBlot Gel Transfer Device (Invitrogen), the membrane was blocked with 5% bovine serum albumin in TTBS buffer (Tris-buffered saline, BioRad; with 0.1% Tween-20). Membranes were incubated with primary antibodies against LMNB1 (#332000, raised in mouse, Invitrogen; used at 1000-fold dilution) or MYH1/2/4/6 (sc-32732, raised in mouse, Santa Cruz; used at 1000-fold dilution) at 4 °C overnight. After washing, the membrane was incubated with 2000-fold diluted anti-mouse HRP-conjugated IgG (GE Healthcare), at room temperature for 1 hour. The blot was developed with ChromoSensor (GenScript) for 3 min at room temperature. Blot images were obtained using a Hewlett-Packard Scanjet 4850. Densitometry was performed using ImageJ (version 1.45, National Institutes of Health). Immunoblots were performed in triplicate, and the mean MYH6 densitometry results normalized to LMNB1 values were reported ± SEM.

Micropipette aspiration of tissues Micropipettes were pulled from glass capillaries (World Precision Instruments, Sarasota, FL) with 1 mm inner diameters using a Flaming-Brown Micropipette Puller (Sutter Instrument, Novato, CA). Pulled tips were scored with the tapered base of another pulled pipette and broken to final inner diameters of 35-45 μm. Pipettes were filled with PBS and attached to water-filled manometer-double reservoir set-up as described elsewhere [S2]. Aspiration was performed at room temperature in PBS supplemented with 3% BSA, without Ca^{2+} to suppress beating. Before each experiment, we incubated the pipette tip in PBS/BSA solution for ≥20 min to prevent tissue sticking inside the pipette. During aspiration, ≥ 3 different pressures were applied from 0.5 – 1.4 kPa for neural tissue and 0.5-20 kPa for cardiac tissue. Aspiration experiments were imaged using a Nikon TE300 microscope with a 20x air objective and recorded using a Cascade Photometric CCD camera. The effective Young's modulus E_t of the local tissue was obtained from the linearity between the difference between the applied pressure inside the pipette relative to outside (ΔP) and strain L/R_p: $\Delta P = \frac{2\pi}{3\Phi_o} E_t \frac{L}{R_p}$, where L is the length of tissue aspirated measured from the mouth of the pipette, R_p is the pipette's inner radius, and φ_o is a shape factor ~2 [S3].

Cell mechanosensitivity assay We isolated cells from heart tissue by dicing to sub-millimeter size and then digesting with Trypsin/EDTA (Gibco, 25200-072). To digest, we incubated tissue in approximately 1 mL Trypsin per E4 HT for 13 min rotating at 37˚C, for 2 min upright to let large tissue pieces settle before carefully removing supernatant and replacing with an equal volume of fresh Trypsin, and finally shaking for 15 more min. We stop digestion by adding an equal volume of chick heart media. Cells were plated at concentrations of approximately 2x10^5 cells/cm directly on collagen I coated PA gels of varying stiffness [S4]. E7 cells were preplated for 2 hours on tissue culture plates to allow fibroblasts to adhere before removing medium with nonadherent cells and plating those cells on collagen I coated PA gels. Spontaneously beating cells were imaged using a Olympus I81 microscope with a 40x air objective configured for phase contrast after 24 hrs in culture, and recorded using a CCD camera at 23 frames/sec. Movies were analyzed using a custom Matlab program to segment cells and track cell area and aspect ratio using the Matlab regionprops function.Strain was calculated for 3 sets of 3 hand-selected seed edge points that were subsequently automatically tracked with a custom Matlab tracking program during beating. The 2D plane strain tensor was calculated for each set of 3 points, throughout and the maximal trace of the strain tensor during contraction was calculated as a measure of strain for a given beat. For each cell, at least 5-10 beats were analyzed. Results were pooled from 4 separate experiments of E4 cardiomyocytes beating on 0.3, 0.9, 2.5, 10, and 40 kPa gels (n = 15, 38, 32, 15, 8).

Latrunculin Recovery Assay E7 cardiomyocytes were cultured on 11 kPa PA gels for 16 hrs. Cells were treated with 20 μM lat-A. After 30 minutes, lat-A was removed. CMs were allowed to recover for 24 hours. In experimental samples (n = 32), 25 μM blebbistatin was added to the media during the full recovery time. In control samples (n = 9), CMs recovered in the presence of plain media. Premyofibril formation was measured by immunofluorescence of sarcomeric α-actinin and non-muscle myosin IIb, where s-α-actinin spacing less than 1.7 ± 0.02 μm or the presence of NMMIIb within striated patterns indicated premyofibril areas.

Whole heart tube transfection Lipofectamine/plasmid complexes were prepared as prescribed by the manufacturers (Lipofectamine 2000, Invitrogen). In particular, for each final 1 mL of transfection solution, 3-4 micrograms of plasmid (GFP or SIRPA-GFP [S5]) and 10 μL Lipofectamine were each diluted to total volumes of 50 μL in Opti-MEM (Gibco, 31985-070) and stayed at room temperature for 5 min before combining both solutions to make the final transfection solution which again sat at room temperature for an additional 25 min. Heart tubes were preincubated in 0.9 mL pre-warmed chick heart media during

lipofectamine/plasmid complex formation. The lipofectamine/plasmid complex was added to the heart tubes in heart media and left to incubate at 37˚C 5% CO_2 for 8-12 hours. Transfection media was replaced with prewarmed chick heart media and the heart tubes continued incubating until use in stiffening or softening experiments and subsequent imaging.

Tissue softening and stiffening treatments To soften collagenous ECM, tissue was incubated in solutions of Collagenase (Type XI, Sigma, C7657) in heart media at 37˚C for the specified amounts of time, and rinsed 2x in heart media for 2 min each. Excised E4 HTs were incubated in 1.0 mg/ml, 0.3 mg/ml or 0.1 mg/ml Collagenase for 30 min. Excised E6 HTs were incubated in 0.3 mg/ml collagenase for the short periods (10-30 min) and long (50 min). To stiffen, E4 tissue was incubated in 20 mg/mL transglutaminase (Sigma, T5398) in chick heart media for 1 hr or 2 hrs at 37˚C (n = 3, 5, respectively, over 2 experiments). Micropipette aspiration was used to measure stiffness of E4 heart tissue before treatment and after 1 hour and 2 hours transglutaminase treatment (n = 2, 2, respectively) in coincidence with untreated controls (n = 1, 1)(Fig. S2A) Similarly, micropipette aspiration was used to measure softening of E4 HTs before and after 1.0, 0.3, and 0.1 mg/ml collagenase treatment(n = 2, 3, 2) (Fig. S2B). For blebbistatin softening experiments, tissue was incubated in 20 μg/ml blebbistatin (EMD Millipore, 203390, stock solution 50 mg/ml in DMSO) in heart media for 30 min at 37 ˚C, and compared to a control of equal concentration of DMSO in heart media.

Heart beat imaging and analysis GFP-transfected E4 chick hearts were imaged while beating by an Olympus I81, using 4x magnification, with phase-contrast and fluorescent illumination and movies were recorded using a CCD camera at rate of of 23 and 17 fps, respectively. To calculate strain, ≥2 groups of 3 cells located within 20 microns of each other were hand chosen along the outer wall of anatomical region of interest (atrium, ventricle, or OFT) along the heart tube. The same procedure and Matlab program were used to track cells and calculate 2D strain as was used to calculate cell-edge strain for cells on gels. Unless HTs were not beating, strain was measured and averaged for at least 5 beats. The velocity of the contraction wave was calculated by dividing the distance along the heart tube between two groups of analyzed cell groups by the time difference their points of peak strains. To visualize cellular calcium, hearts were loaded with Fluo-4 AM (Fluo-4 AM F14217, Life Technologies) for 30 min at room temperature prior to imaging, following the manufacturer's protocol.

Myofibril striation imaging and analysis To visualize myofibril structure and organization in intact heart tubes and isolated cardiomyocytes, we stained samples for sarcomeric a-actinin-2, filamentous actin (TRITC-phalloidin, Life Technologies) and DNA (Hoechst 33342). Isolated cardiomyocytes and whole heart tubes were first incubated in relaxing buffer [S6] for 5 min and 20 min, then fixed in 4% Formaldehyde for 5 min and 20 min, respectively. They were then rinsed three times in blocking buffer (3% BSA in PBS), then left in blocking buffer for 1 hr at room temperature. Samples were incubated in sarcomeric a-actinin-2 primary antibody (1:500 in blocking buffer) overnight at 4˚C rocking. They were again rinsed 3x in blocking buffer before incubating in secondary antibody (1:1000 in blocking buffer) with TRITC-phalloidin (1:2000). Finally, samples were incubated 10 min in Hoechst 33342 (1:1000) in blocking buffer and mounted with mounting medium. Cells on gels were mounted on coverslips and sealed with clear nail polish imaged by wide-field fluorescence imaging with a 60x oil-objective. All striated fibers were hand traced, and striation spacing was measured as the distance between peaks of the α-actinin image by a peakfinder program in Matlab. Z-disc breadth was measured as the FWHM of the intensity profile perpendicular to the local myofibril direction, after subtracting the best fit linear trend line. Histograms of striation spacing for cells on gels fit to a bimodal: count = $a*\exp(-(s-\mu_p)^2/2\sigma_p^2 + b*\exp(-(s-\mu_m)^2/2\sigma_m^2$ where s is the striation spacing bin, and a, b, μ_p, μ_m, σ_p, σ_m are best

fit parameters. Relative premyofibril and myofibril fractions of a/(a+b) and b/(a+b) ± least squares fit error are respectively in Fig. 4E, and premyofibril and myofibril spacing respectively are $\mu_p \pm \sigma_p$ and $\mu_m \pm \sigma_m$, in Fig. 4D. To estimate the average z-disc breadth of premyofibrils vs. myofibrils, we took the striations with spacing ≤ 1.3 μm to be premyofibrils and ≥ 1.8 μm to be myofibrils and reported the mean ± SEM z-disc breadth associated with each respective population. Whole untreated and treated HTs were imaged on a Zeiss LSM 710 confocal with a 40x air-obective, with z-plane spacing of 0.48 μm. Striation in intact heart was analyzed using ImageJ. We converted the z-stack to a stack with z-plane spacing 0f 1.96 by grouped average intensity z-projections of every 4 images. For a given z-plane, we selected 5 random in-plane, unbranched sections of myofibrils at least 20 μm long using a random number generator to choose 5 random x-y coordinates from which we found the nearest candidate myofibrils. We used planes 6, 16, and 26 μm into the ventricular tissue of untreated (n = 2 HT, m = 479 z-discs) and 0.3 mg/ml collagenase softened (n = 2 HT, m = 479 z-discs) E4 HT. Z-disc spacing and breadth were calculated as described for myofibrils in the cells on gels. The mean of all individual spacings and breadths ± SEM were taken for each condition.

Supplemental References

[S1] J. Shin, J. Swift, K. Spinler and D. Discher, "Myosin-II inhibition and soft 2D matrix maximize multinucleation and cellular projections typical of platelet-producing megakaryocytes," ***PNAS,*** vol. 108, pp. 11458-11463, 2011.

[S2] K. N. Dahl, S. M. Kahn, K. L. Wilson and D. E. Discher, "The nuclear envelope lamina network has elasticity and a compressibility limit suggestive of a molecular shock absorber," ***Journal of Cell Science,*** vol. 117, pp. 4779-4786, 2004.

[S3] D. Theret, M. Levesque, M. Sato, R. Nerem and L. Wheeler, "The application of a homogeneous half-space model in the analysis of endothelial cell micropipette measurements," ***Journal of Biomechanical Engineering,*** vol. 110, pp. 190-199, 1988.

[S4] A. Engler, C. Carag-Krieger, C. Johnson, M. Raab, H. Tang, D. Spelcher, J. Sanger, J. Sanger and D. Discher, "Embryonic cardiomyocytes beat best on a matrix with heart-like elasticity: scar-like rigidity inhibits beating," ***Journal of Cell Science,*** vol. 10, no. 24, pp. 3794-3802, 2008.

[S5] P. Rodriguez, T. Harada, D. Christian, D. Pantano, R. Tsai and D. Discher, "Minimal "self" peptides that inhibit phagocytic clearance and enhance delivery of nanoparticles," ***Science,*** vol. 339, no. 6122, pp. 971-075, 2013.

[S6] Y. Ono, C. Schwach, P. Antin and C. Gregorio, "Disruption in the tropomodulin1 (Tmod1) gene compromises cardiomyocyte development in murine embryonic stem cells by arresting myofibril maturation," ***Developmental Biology,*** vol. 282, no. 2, pp. 336-348, 2005.

[S7] P. Devreotes, "Dictyostelium discoideum: a model system for cell-cell interactions in development," ***Science,*** vol. 245, no. 4922, p. 1054, 1989.

[S8] P. Gillespie and R. Walker, "Molecular basis of mechanosensory transduction," ***Nature,*** vol. 413, no. 6852, pp. 194-202, 2001.

[S9] C. Kung, "A possible unifying principle for mechanosensation," ***Nature,*** vol. 436, pp. 647-654, 2005.